

Engineering a pyrene MOF composite photocatalyst toward the formation of carbon dioxide radical anion through regulating the charge transfer from type-II to Z-scheme via a chemical bond-modulated strategy

Xin Zhao,^a Yajun Zhao,^a Yuan-Peng Li,^a Pengbo Lyu,^{*c} Chunying Chen,^d Zong-Wen Mo,^{a,b} Chao Peng,^{a,b} Jiewei Liu^{*a,b} and Li Zhang^{*d}

^a School of Environmental and chemical Engineering, Jiangmen Key Laboratory of Synthetic Chemistry and Cleaner Production, Institute of Carbon Peaking and Carbon Neutralization, Wuyi University, Jiangmen 529020, P.R. China. E-mail addresses: wyuchemliujw@126.com

^b Guangdong Provincial Laboratory of Chemistry and Fine Chemical Engineering Jieyang Center, Jieyang 515200, China.

^c Hunan Provincial Key Laboratory of Thin Film Materials and Devices, School of Materials Science and Engineering, Xiangtan University, Xiangtan 411105, China. E-mail addresses: pengbo.lyu@xtu.edu.cn

^d School of Chemistry, Sun Yat-Sen University, Guangzhou 510006, China. E-mail addresses: zhli99@mail.sysu.edu.cn

Contents

1. General Information	S5
2. Experimental section.....	S6
3. Characterization of the photocatalysts	S8
4. Photocatalytic Cyclization of Propargylic Amines with CO ₂	S15
5. Reaction mechanism study	S21
6. Characterizations of propargylic amines and oxazolidinones	S23

Captions for Figures and Tables

Figure S1. PXRD patterns of WYU-11, CdS, CdS@WYU-11 and CdS@WYU-11-Cys composites.

Figure S2. PXRD patterns (a), SEM (b), TEM (c), XPS patterns (d) and EDS elemental mapping images (e) of WYU-11-Cys, respectively.

Figure S3. TEM images of CdS@WYU-11-Cys.

Figure S4. High resolution TEM images of CdS@WYU-11 and the size distribution of CdS (left); The lattice fringe of the CdS (right).

Figure S5. N₂ adsorption-desorption isotherm of WYU-11, CdS@WYU-11 and CdS@WYU-11-Cys composites at 77 K.

Figure S6. UV-vis DRS of WYU-11, CdS, CdS@WYU-11 and CdS@WYU-11-Cys composites.

Figure S7. Tauc plot of WYU-11 (a) and CdS (b); Mott-Schottky plot of WYU-11 (c) and CdS (d) in a 0.1 M Na₂SO₄ solution containing K₃Fe(CN)₆/K₄Fe(CN)₆ (0.01 M).

Figure S8. Band structure of WYU and CdS.

Figure S9. Scheme illustrating the potential type II or Z-scheme charge transfer pathways between WYU-11 and CdS in the CdS@WYU-11-Cys composites.

Figure S10. S 2p of CdS@WYU-11-cys composite in the dark and under visible light irradiation ($\lambda > 400$ nm).

Figure S11. VB-XPS of (a)WYU-11, (b) CdS and (c) WYU-11-Cys, respectively.

Figure S12. The cycling experiments of CdS@WYU-11-Cys for the photocatalytic cyclization of CO₂ and propargylic amines.

Figure S13. The SEM images of CdS@WYU-11-Cys before (a) and after (b) photocatalysis.

Figure S14. The TEM image of CdS@WYU-11-Cys after the second run.

Figure S15. The PXRD patterns of CdS@WYU-11-Cys before and after catalytic reaction.

Figure S16. XPS spectrum of CdS@WYU-11-Cys before and after catalytic reaction.

Figure S17. The cysteamine-grafted configuration and adsorption of *N*-benzylprop-2-yn-1-amine configuration within WYU-11. The distances are in Å.

Figure S18. CO₂ isotherms of Cds@WYU-11-Cys at different temperatures.

Figure S19. The photocatalytic cyclization reaction of propargylic amine with CO₂ in the presence of MeOH or K₂S₂O.

Figure S20. The optimized crystal structure (double-cell) in dehydrated form viewing along (a) *a*

(14.24 Å), (b) **b** (11.14 Å) and (c) **c** (32.26 Å) directions.

Table S1. EXAFS fitting parameters of the Cd *K*-edge towards WYU-11-Cys.

Table S2. Control experiments for the photocatalytic cyclization reaction of propargylic amine (**1a**) with CO₂.

Table S3. Solvent optimization for the photocatalytic cyclization reaction of propargylic amine (**1a**) with CO₂.

Table S4. Comparison of CdS@WYU-11-Cys and other MOF-based catalysts for the cyclization reaction of propargylic amine with CO₂.

1. General information

All reagents and solvents used in this work were purchased from commercial supplies without further purification. Powder X-ray diffraction (PXRD) studies were carried out on a Rigaku MiniFlex 600-C diffractometer (Bragg-Brentano geometry, Cu-K α radiation, $\lambda = 1.54178 \text{ \AA}$). ^1H NMR was recorded on Bruker AVANCE III 500(500 MHz). XPS analyses were performed on a Thermo Scientific ESCALAB 250Xi with a monochromatized micro-focused Al K α X-ray source provided by eceshi (www.eceshi.com). Binding energies (BE) were calibrated by setting the measured BE of C 1s to 284.65 eV. UV-vis absorption spectra were recorded on a Shimadzu UV-3600 Plus spectrometer. Fluorescence spectra were measured on an Edinburgh FLS1000 Photoluminescence Spectrometer. The fluorescence lifetime experiments were performed in the time-correlated single photo counting (TCSPC) methods by using 340 nm picoseconds pulsed diode laser. The sorption isotherms were measured with an ASAP 2460/2020 gas sorption analyzer. Scanning electron microscopy (SEM) analysis was performed using a Zeiss Gemini SEM 500 apparatus. Transmission electron microscopy (TEM) investigations was performed by Tecnai G2 F20 S-TWIN. High-angle annular dark-field scanning TEM (HAADF-STEM) was performed by Thermo Scientific Themis Z. Samples for SEM tests were dispersed in EtOH with the aid of sonication, and then deposited on a conductive tape. Prior to TEM measurements, samples were dispersed in ethanol using a sonication method, and then mounted on a carbon coated copper grid.

2. Experimental section

2.1 Synthesis of CdS particles

Typically, $\text{Cd}(\text{CH}_3\text{COO})_2 \cdot 2\text{H}_2\text{O}$ (133.3 mg, 0.5 mmol) is added into 20 mL of dry ethanol, then the whole mixture are kept stirring and reflux at 80 °C for 12 h. The CdS particles are separated by centrifugation and washed with distilled water for several time and dried under vacuum at 60 °C overnight.

2.2 Photoelectrochemical characterization

Photoelectrochemical measurements were performed on a CHI 660E electrochemical work station (Chenhua Instrument, Shanghai, China) in a standard three-electrode system with the sample-coated FTO, Pt plate and Ag/AgCl as the working electrode, counter electrode and reference electrode, respectively. The as-synthesized samples (5 mg) were added into Dupont D520 Nafion (25 μL) and ethanol (0.2 mL) mixed solution, giving a suspension, and then the working electrodes were prepared by dropping the suspension onto the surface of a FTO plate. The working electrodes were dried at room temperature. The photocurrent was measured using constant voltage tracking (CVT) using a 0.1 M Na_2SO_4 solution containing $\text{K}_3\text{Fe}(\text{CN})_6/\text{K}_4\text{Fe}(\text{CN})_6$ (0.01 M) as the electrolyte. A 300 W Xe lamp ($\lambda \geq 400$ nm) was used as the light source, and a shutter was used to modulate the light and dark conditions during the test. Photo-responsive signals of the samples were measured under chopped light at 10^{-5} V. The electrochemical impedance spectroscopy (EIS) was performed in frequency range from 10^{-2} to 10^3 Hz with a bias potential of 0.005 V. The Mott-Schottky measurements were performed at frequencies of 500, 1000, and 1500 Hz, respectively.

2.3 In situ irradiated X-ray photoelectron spectroscopy (ISI-XPS)

In situ irradiated X-ray photoelectron spectroscopy (XPS) measurements were conducted on a Thermo Scientific ESCALAB 250Xi with a monochromatized micro-focused Al Ka X-ray source. All binding energies were referenced to the adventitious C 1s line at 248.4 eV. A 300 W Xe lamp ($\lambda \geq 400$ nm) (Perfect Light) was kept ≈ 15 cm away from the samples as a light source.

2.4 EPR radicals trapping experiments

The spectra were collected from a Bruker EMXnano spectrometer at room temperature using 5,5-Dimethyl-1-pyrroline N-oxide (DMPO) as radical trapping agent. The DMPO- $\bullet\text{CO}_2^-$ adduct was obtained from the mixing of 20 μL solution A (10 mg of the sample powder dispersing in 2 mL CH_3CN) and 20 μL solution B (20 μL of DMPO added into 200 μL CH_3CN), which was irradiation under atmospheric CO_2 and visible light ($\lambda \geq 400$ nm) for 5 min.

3. Characterization of the photocatalysts

Table S1. EXAFS fitting parameters of the Cd *K*-edge towards WYU-11-Cys

Sample	Path	CN	$R/\text{\AA}$	$\sigma^2(\text{\AA}^2)$	$\Delta E_0(\text{eV})$	<i>R</i> factor
CdO	Cd–O	5.9	2.34	0.009	3.8	0.01
	Cd–O–Cd	12.4	3.32	0.003	1.45	
WYU-11-Cys	Cd–O/Cd–N	4.9	2.29	0.007	13.2	0.004

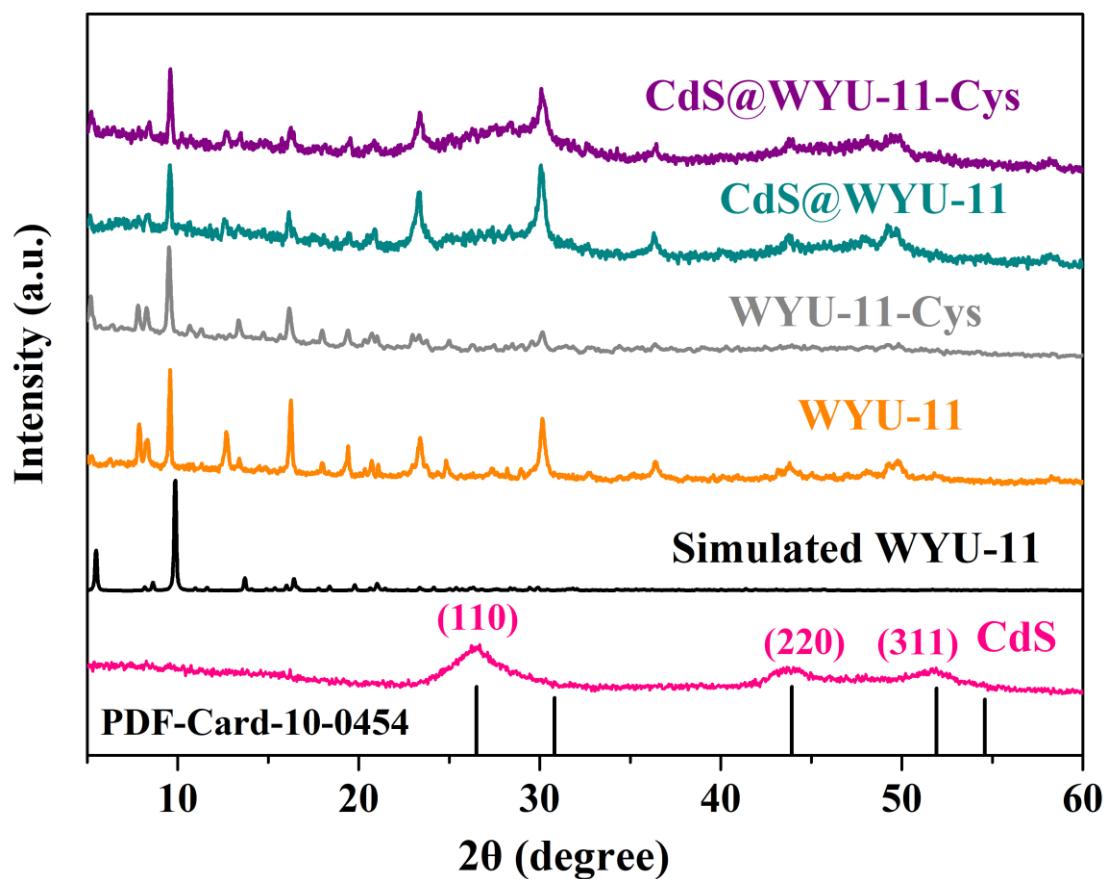


Figure S1. PXRD patterns of CdS, WYU-11, WYU-11-Cys, CdS@WYU-11 and CdS@WYU-11-Cys composites.

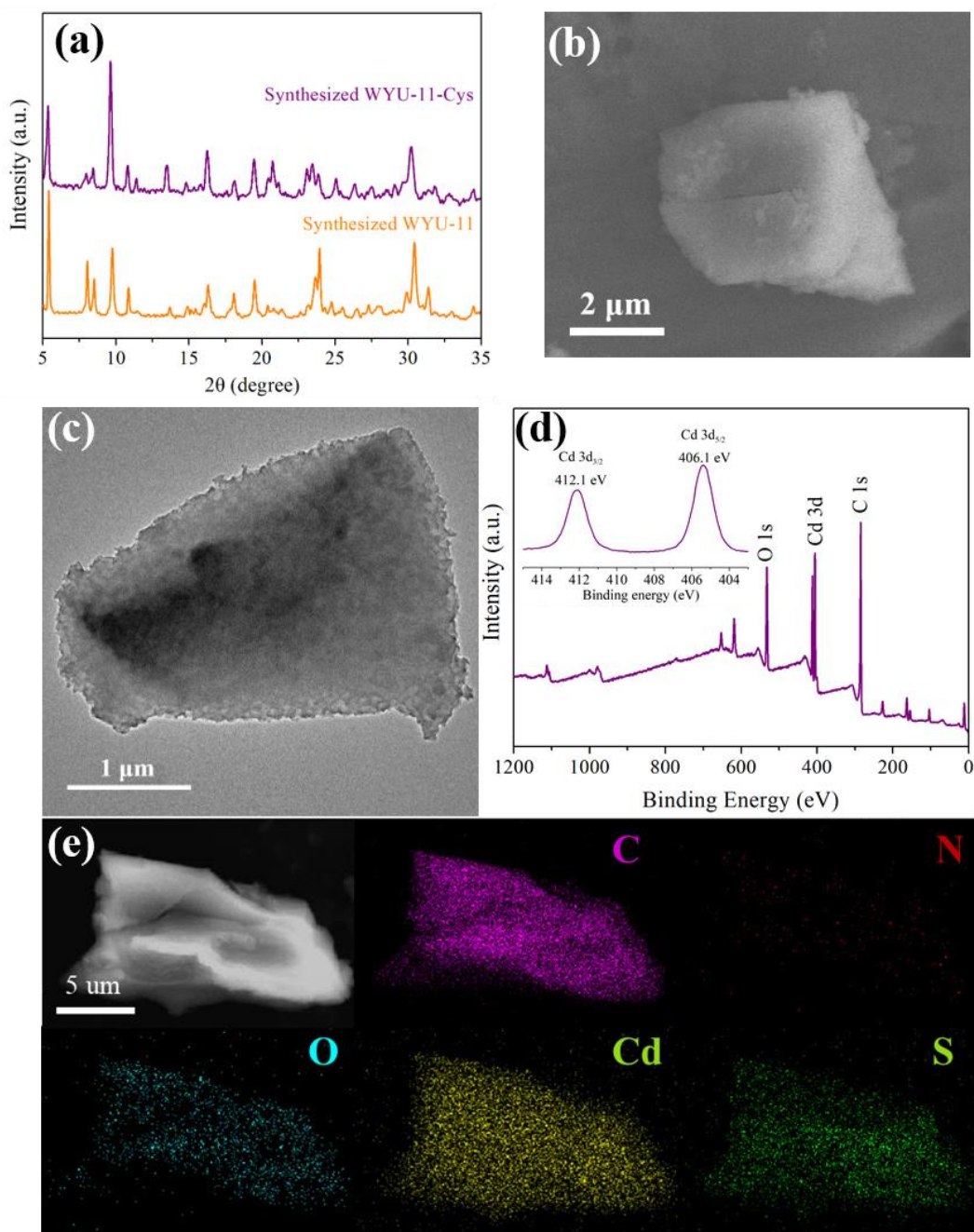


Figure S2. PXRD patterns (a), SEM (b), TEM (c), XPS spectrum (d) and EDS elemental mapping images (e) of WYU-11-Cys, respectively.

The bulk purity and irregular morphology of WYU-11-Cys were revealed by the PXRD patterns (Figure S2a), scanning electron microscopy (SEM) (Figure S2b) and TEM (Figure S2c). XPS spectrum indicates of the +3 valence nature of Cd in WYU-11-Cys (Figure S2d). EDX elemental mapping images indicated the evenly distribution of all the elements in the whole WYU-11-Cys material (Figure S2e).

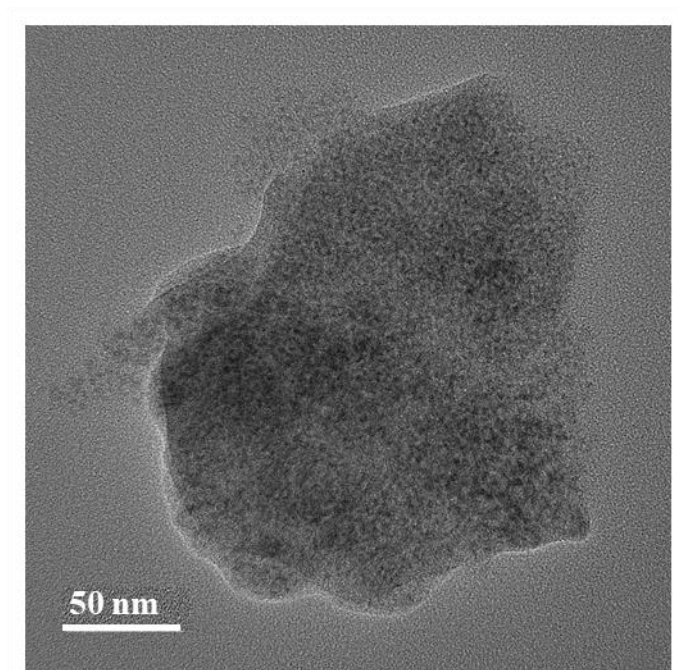


Figure S3. TEM images of CdS@WYU-11-Cys.

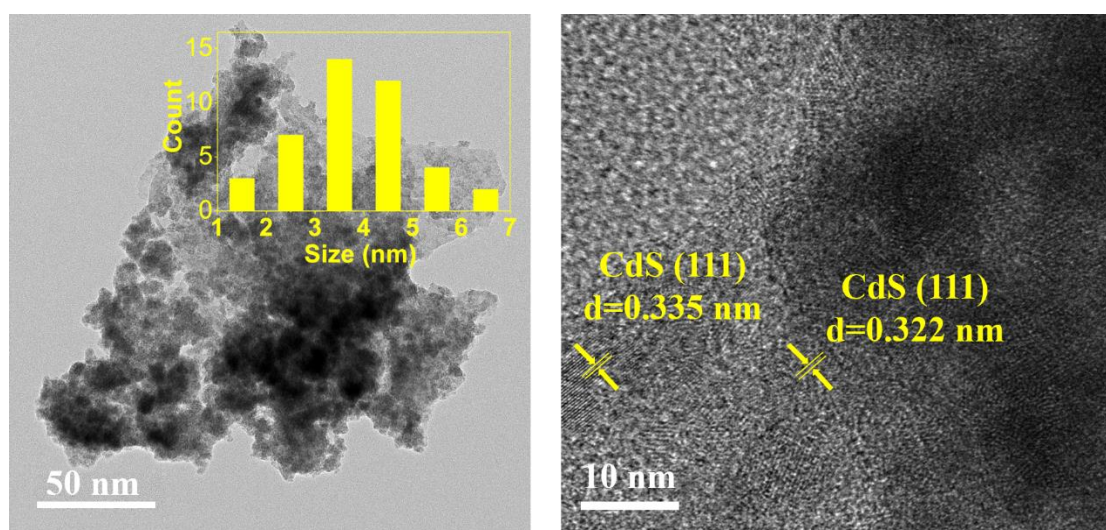


Figure S4. High resolution TEM images of CdS@WYU-11 and the size distribution of CdS (left);
The lattice fringe of the CdS (right).

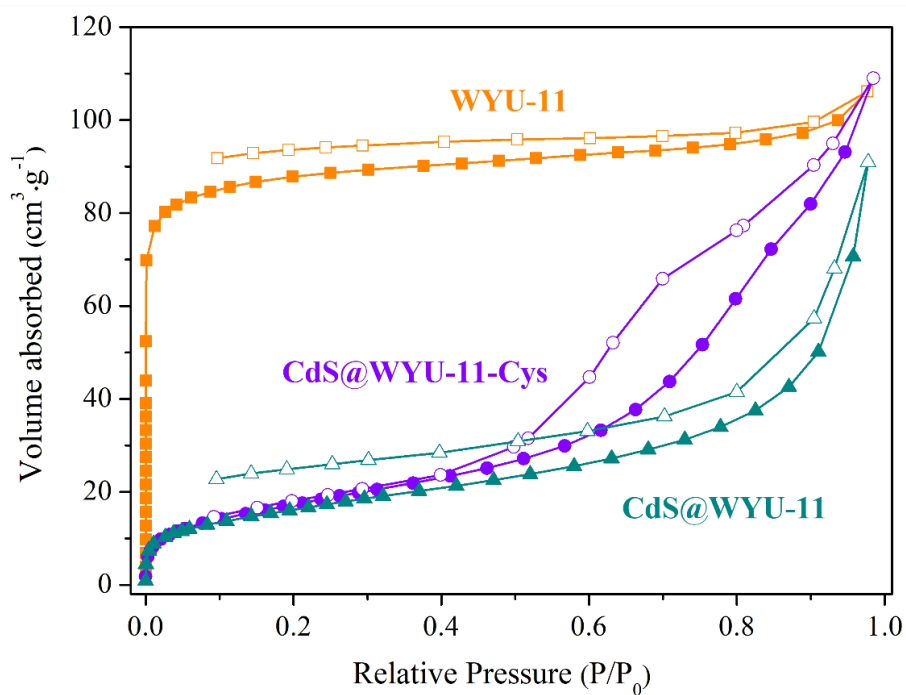


Figure S5. N₂ adsorption-desorption isotherm of WYU-11, CdS@WYU-11 and CdS@WYU-11-Cys composites at 77 K.

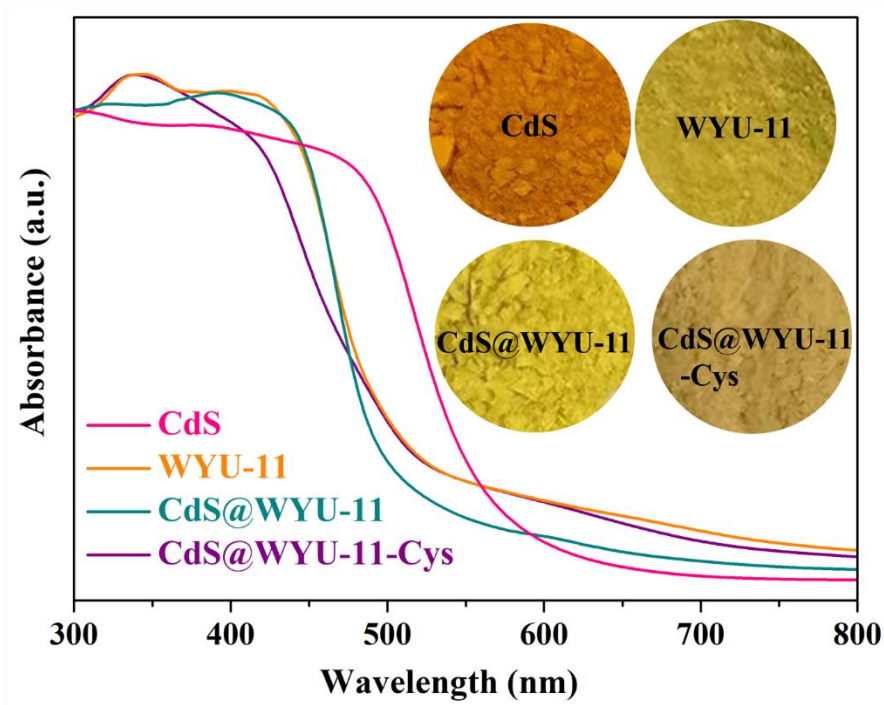


Figure S6. UV-vis DRS of WYU-11, CdS, CdS@WYU-11 and CdS@WYU-11-Cys composites.

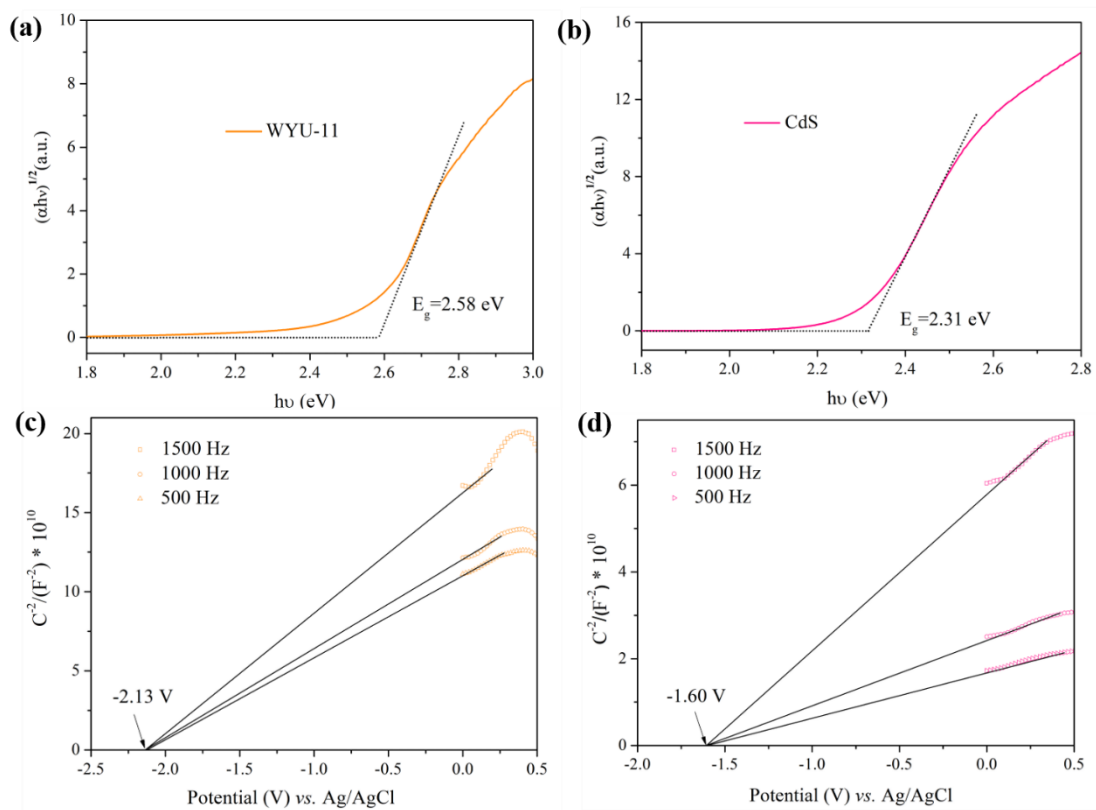


Figure S7. Tauc plot of WYU-11 (a) and CdS (b); Mott-Schottky plot of WYU-11 (c) and CdS (d) in a 0.1 M Na₂SO₄ solution containing K₃Fe(CN)₆/K₄Fe(CN)₆ (0.01 M).

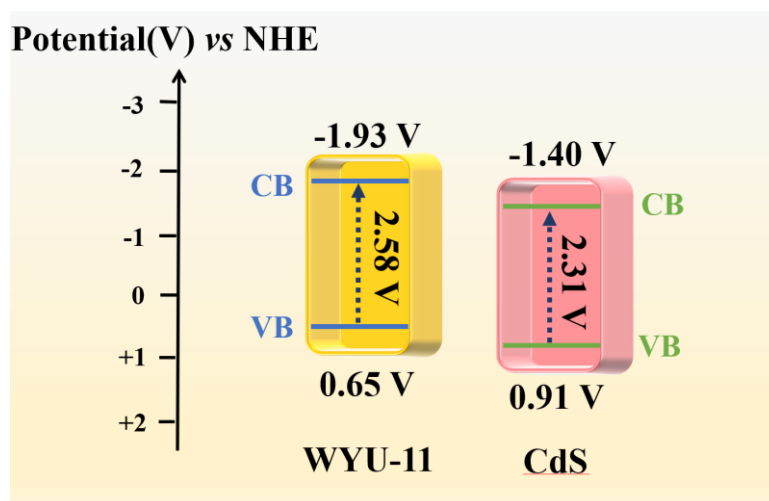


Figure S8. Band structure of WYU and CdS.

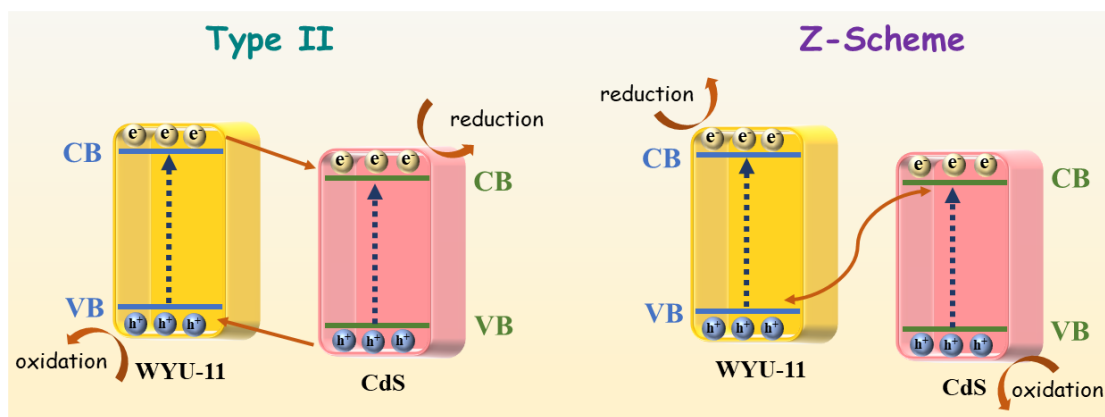


Figure S9. Scheme illustrating the potential type II or Z-scheme charge transfer pathways between WYU-11 and CdS in the CdS@WYU-11-Cys composites.

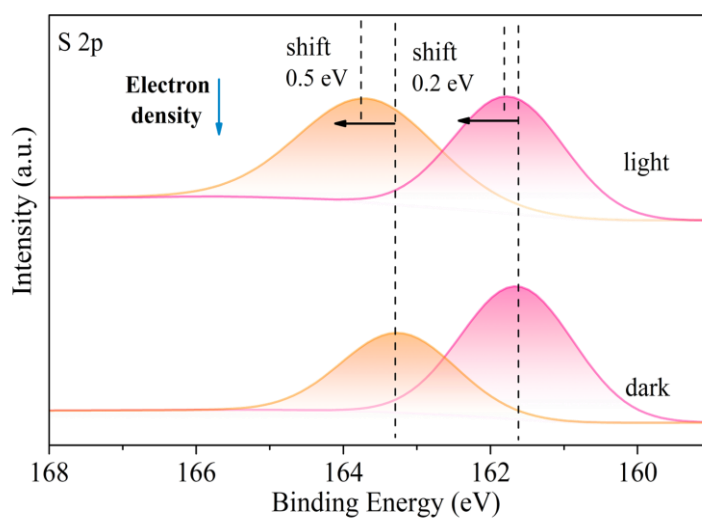


Figure S10. (h) S 2p of CdS@WYU-11-cys composite in the dark and under visible light irradiation ($\lambda > 400$ nm).

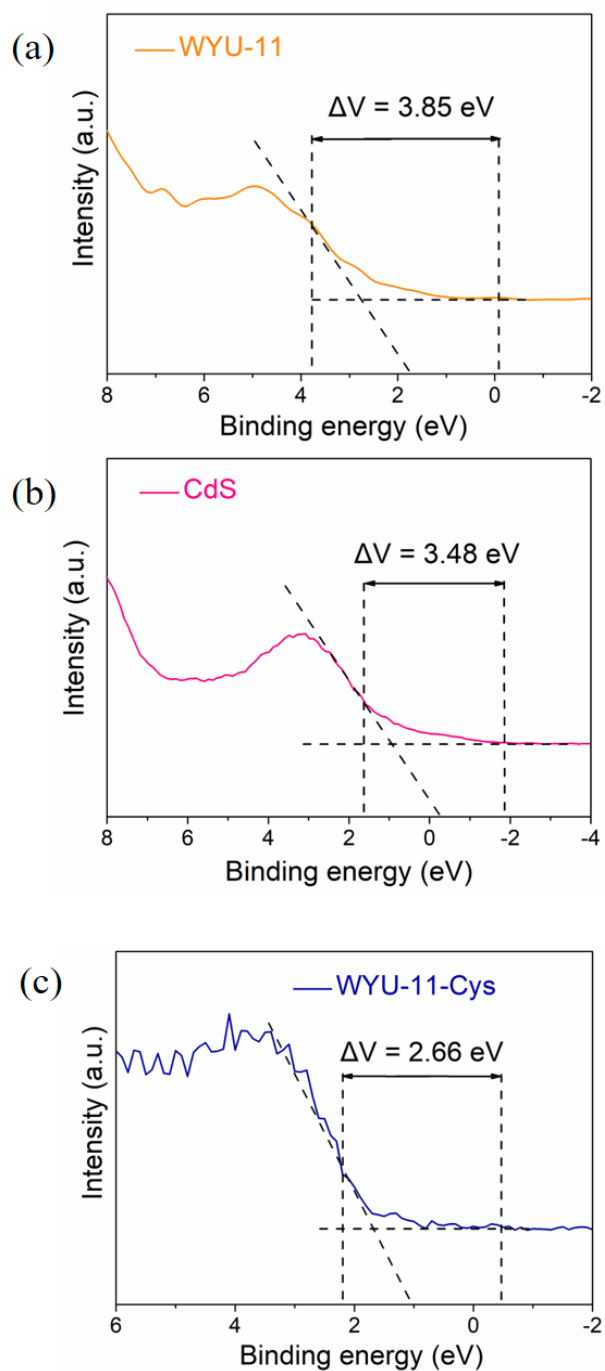
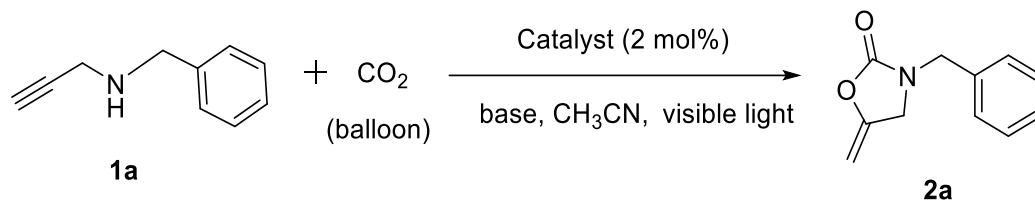


Figure 11. VB-XPS of (a)WYU-11, (b) CdS and (c) WYU-11-Cys, respectively.

The work functions (Φ) were calculated by the valence band X-ray photoelectron spectroscopy (VB-XPS) method based on the equation: $\Phi = \phi + \Delta V$ (ϕ represents work function of XPS analyzer, $\phi = 4.2 \text{ eV}$, ΔV is the contact potential difference). The ΔV values were obtained by analyzing the distance between two inflection points (IP) in VB XPS. Therefore, the work functions (Φ) of WYU-11, CdS and WYU-11-Cys were calculated to be 8.05, 7.68 and 6.86 eV, respectively.

4. Photocatalytic Cyclization of Propargylic Amines with CO₂

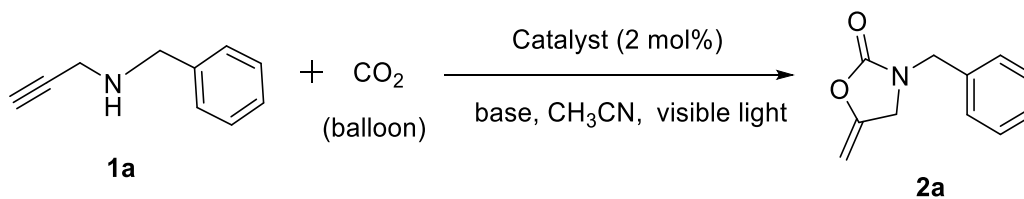
Table S2. Control experiments for the photocatalytic cyclization reaction of propargylic amine (**1a**) with CO₂^a



entry	catalyst	base	yield (%) ^b
1	CdS@WYU-11-Cys	TMG	97
2	CdS@WYU-11	TMG	30
3 ^c	H ₄ PTTB	TMG	trace
4 ^d	CdS	TMG	26
5 ^e	WYU-11	TMG	19
6	none	TMG	0
7	CdS@WYU-11-Cys	none	trace
8 ^f	CdS@WYU-11-Cys	TMG	trace
9 ^g	CdS@WYU-11-Cys	TMG	trace

^a Reaction condition: **1a** (73 mg, 0.5 mmol), Catalyst (2 mol%), TMG (11.5 mg, 0.1 mmol), CH₃CN (2 mL), visible light ($\lambda > 400$ nm), 8 h, CO₂ (balloon). ^b The yield of the reaction was determined by ¹H NMR of the crude residue. ^c 0.01 mmol of H₄PTTB. ^d 0.01 mmol of CdS. ^e 0.01 mmol of WYU-11. ^f N₂ atmosphere. ^g in the absence of visible light irradiation.

Table S3. Base optimization for the photocatalytic cyclization reaction of propargylic amine (**1a**) with CO₂.^a



entry	catalyst	base	yield (%) ^b
1	CdS@WYU-11-Cys	TMG	97
2	CdS@WYU-11-Cys	DBU	91
3	CdS@WYU-11-Cys	DIPEA	6
4	CdS@WYU-11-Cys	TEA	14

^a Reaction condition: **1a** (73 mg, 0.5 mmol), Catalyst (13 mg, 2 mol%), TMG (11.5 mg, 0.1 mmol), CH₃CN (2 mL), visible light ($\lambda > 400$ nm), 8 h, CO₂ (balloon). ^bThe yield of the reaction was determined by ¹H NMR of the crude residue.

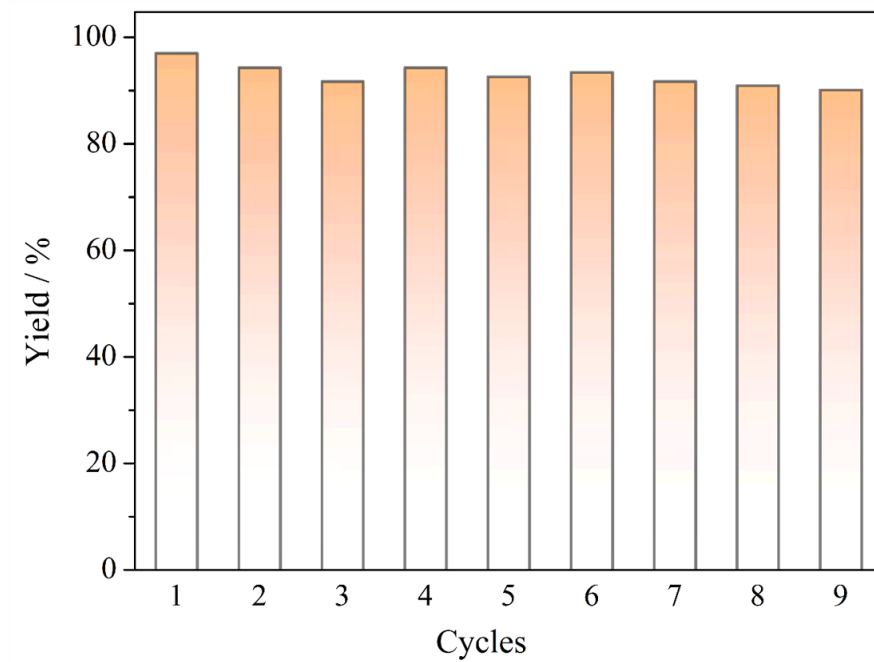
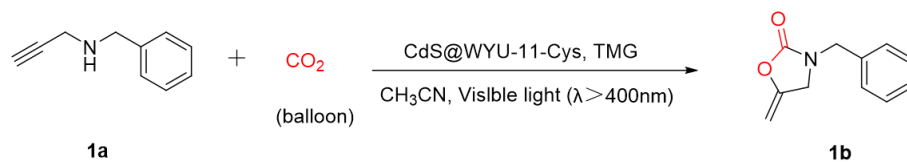


Figure S12. The cycling experiments of CdS@WYU-11-Cys for the photocatalytic cyclization of CO₂ and propargylic amines.

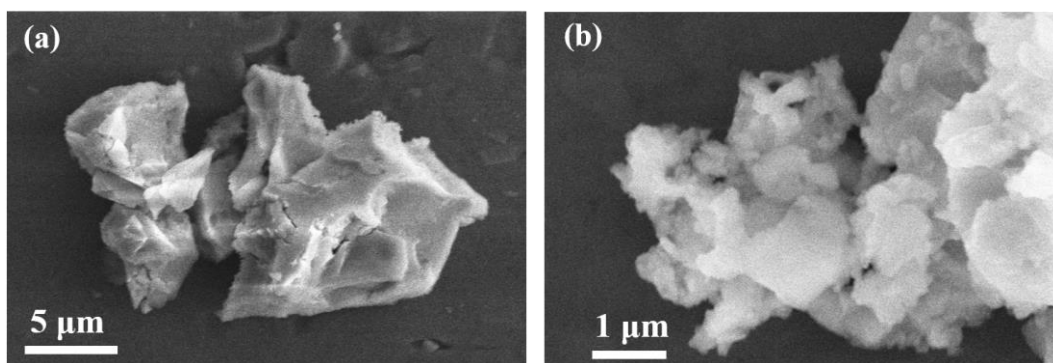


Figure S13. The SEM images of CdS@WYU-11-Cys before (a) and after (b) photocatalysis.

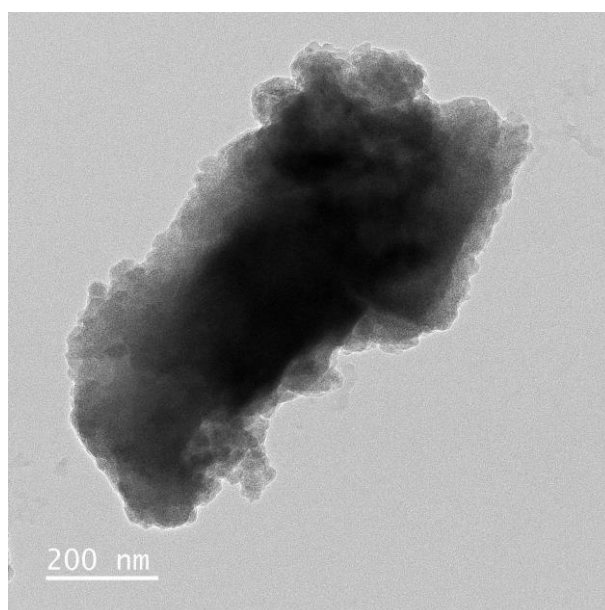


Figure S14. The TEM image of CdS@WYU-11-Cys after the second run.

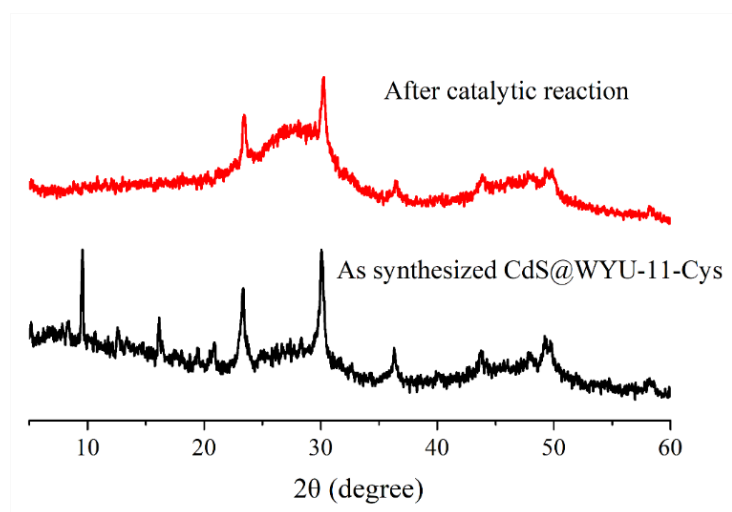


Figure S15. The PXRD patterns of CdS@WYU-11-Cys before and after catalytic reaction.

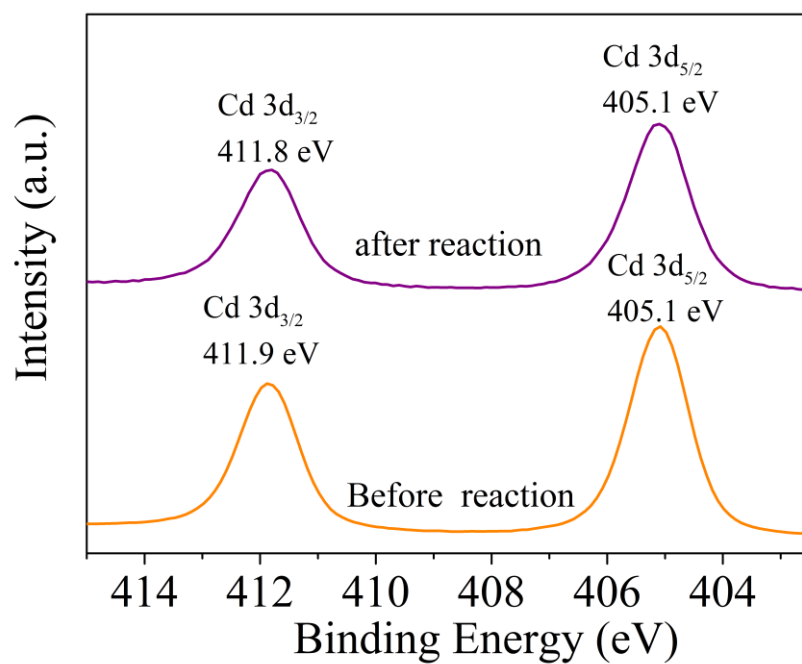


Figure S16. XPS spectrum of CdS@WYU-11-Cys before and after catalytic reaction.

Table S4. Comparison of CdS@WYU-11-Cys and other MOF-based catalysts for the cyclization reaction of propargylic amine with CO₂.

Catalysts	Amount of Catalyst	Visible light	T(°C)	Time(h)	Yield (%)	Reference
Zn ₁₁₆	0.27 mol%	/	70	12	99	<i>Angew. Chem. Int. Ed.</i> , 2020 , <i>132</i> , 8664-8671
MOF-Cu-Mg	1.4 mol%	/	25	6	93	<i>Inorg. Chem.</i> , 2021 , <i>60</i> , 13425–13433
Ag ₂₇ -MOF	1 mol%	/	25	6	97	<i>Angew. Chem. Int. Ed.</i> , 2020 , <i>59</i> , 20031–20036
TNS-Ag8	0.1 mol%	/	25	24	95	<i>ACS Catal.</i> , 2018 , <i>8</i> , 1384–1391
NiBDP-AgS	0.5 mol%	/	25	4	99	<i>ChemComm.</i> , 2018 , <i>54</i> , 4469-4472
TMOF-3-Ag	10 mol%	/	50	12	97	<i>ACS Catal.</i> , 2018 , <i>8</i> , 2519-2525
Ag-MOF-1	4 mol%	/	25	24	95	<i>ACS Omega</i> , 2019 , <i>4</i> , 10828-10833
MOF-SO ₃ Ag	0.15 mol%	/	25	24	99	<i>Inorg. Chem.</i> , 2020 , <i>59</i> , 9765–9773
Cu-TSP	2 mol%	/	50	24	99	<i>Inorg. Chem. Front.</i> , 2022 , <i>9</i> , 3839–3844
Ag@2,6-FPP-TAPT	0.052 mol%	/	50	2	99	<i>Green Chem.</i> , 2022 , <i>24</i> , 930–940
Cu ₂ O@ZIF-8	5 mol%	/	40	6	99	<i>Angew. Chem.</i> , 2022 , e202114817
Cu ₂ O@MIL-101(Cr)-DABCO	2.5 mol%	/	25	12	99	<i>Green Chem.</i> , 2023 , <i>25</i> , 1938–1947
MOF-1a-Cd	0.4 mol%	/	60	24	82	<i>Chemcatchem.</i> , 2017 , <i>9</i> , 4598
WYU-11	1 mol%	/	60	24	99	<i>Inorg. Chem.</i> , 2023 , <i>62</i> , 18553-18562
Cu-TCPP(Fe)	1 mol%	/	50	24	98	<i>Dalton Trans.</i> , 2024 , <i>53</i> , 10060–10064
Cu ^I /Cu ^{II} mixed-valence MOF	0.5 mol%	/	50	12	99	<i>Inorg. Chem. Front.</i> , 2024 , <i>11</i> , 6072-6078
{[Cu ₅ I ₆ Th ₆ (μ ₃ O) ₄ (μ ₃ -OH) ₄ (H ₂ O) ₁₀ (L) ₁₀ }	1 mol%	/	r.t	6	98	<i>Inorg. Chem.</i> , 2024 , <i>63</i> , 13450–13458
1 _{0.1} -2 _{0.4} -3 _{0.5} -JNM	3 mol%	/	r.t	3	99	<i>J. Am. Chem. Soc.</i> , 2024 , <i>146</i> , 19271–19278
Cds@WYU-11-Cys	2 mol%	λ > 400 nm	r. t	8	97	This work

5. Reaction mechanism study

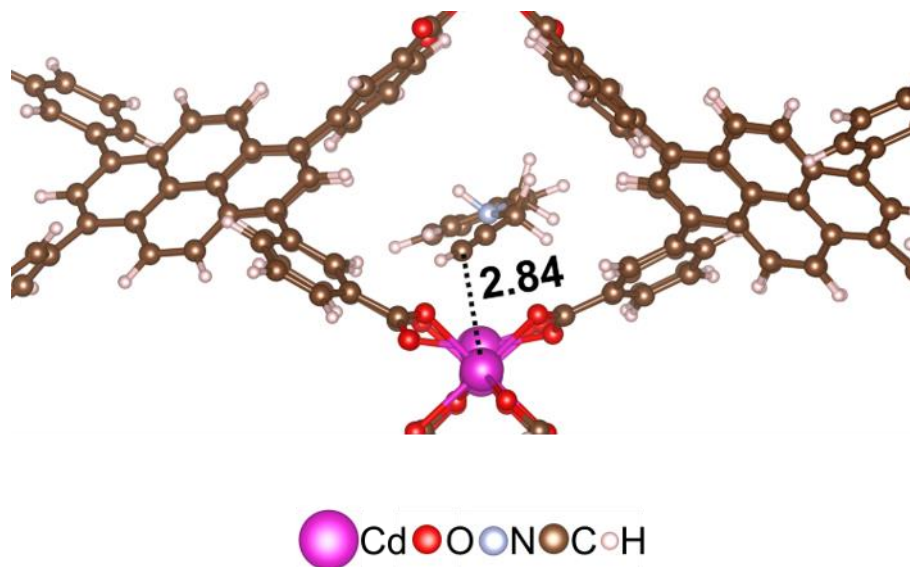


Figure S17. The cysteamine-grafted configuration and adsorption of *N*-benzylprop-2-yn-1-amine configuration within WYU-11. The distances are in Å.

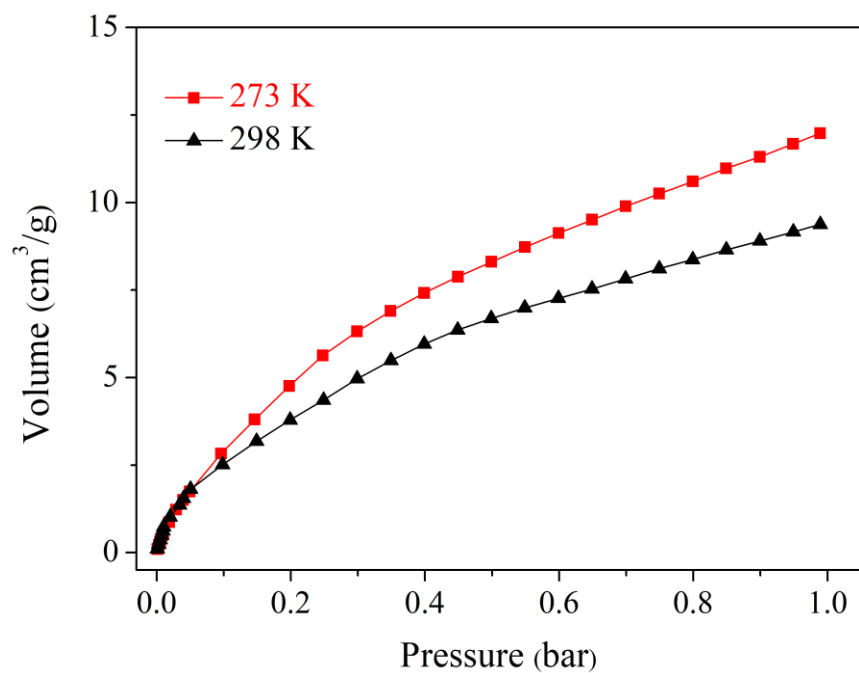


Figure S18. CO₂ isotherms of Cds@WYU-11-Cys at different temperatures.

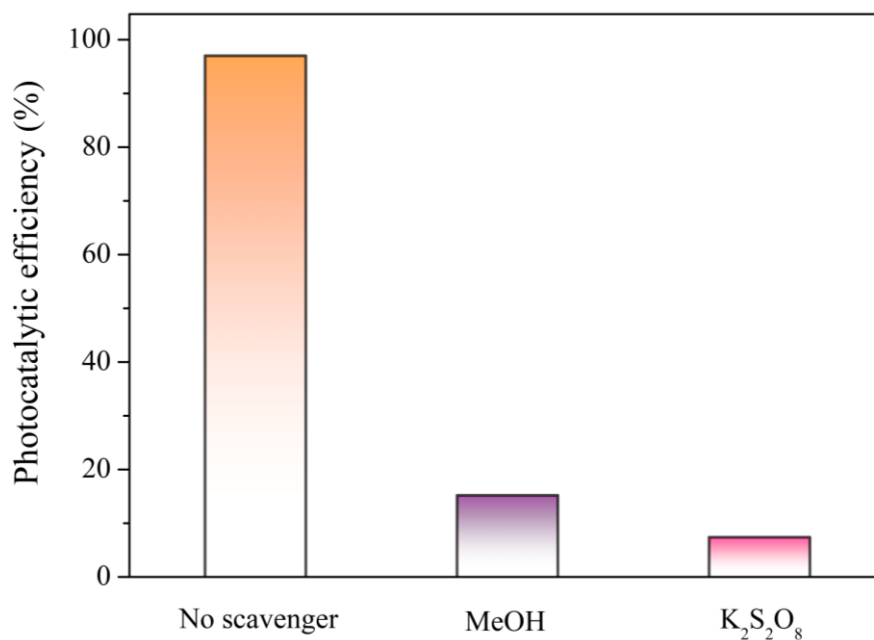


Figure S19. The photocatalytic cyclization reaction of propargylic amine with CO₂ in the presence of MeOH or K₂S₂O₈.

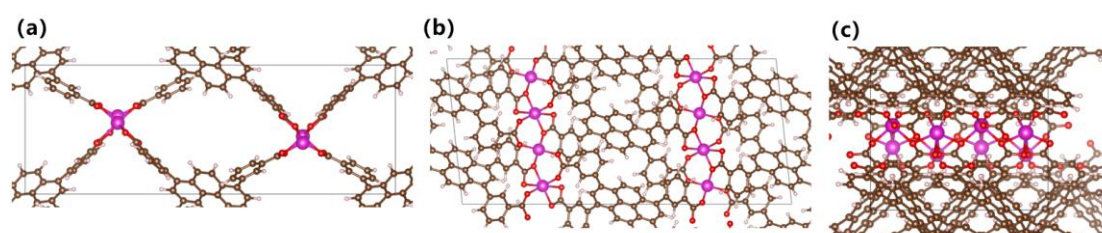
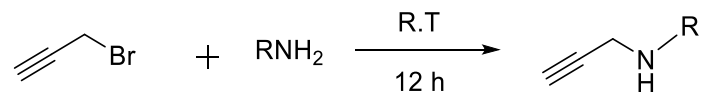


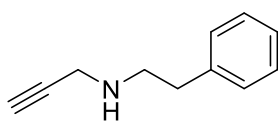
Figure S20. The optimized crystal structure (double-cell) in dehydrated form viewing along (a) *a* (14.24 Å), (b) *b* (11.14 Å) and (c) *c* (32.26 Å) directions.

6. Characterizations of propargylic amines and oxazolidinones

Synthesis of propargylic amines (**1a-11**)

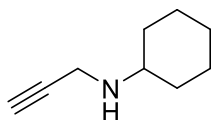


Terminal propargylic amines (**1a-11**) were synthesized according to the previous report.^[1, 3-4] In a typical experiment, propargylic bromide (0.45 mL, 4 mmol) was added into propargylic amine (20 mmol) dropwise via a constant pressure drop funnel over thirty minutes, and stirred overnight for about 12 h at ambient temperature. Then the resulting mixture was diluted in Et₂O and washed with saturated aq. NaHCO₃ (3×10 mL), and dried over anhydrous Na₂SO₄. The reaction mixture was concentrated and purified by column chromatography on silica gel eluting with 10:1 petroleum ether/ethyl acetate to afford the corresponding product as yellow oil.



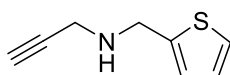
1d

Yellow oil has been obtained after being purified by column chromatography on silica gel (eluting with PE/Ethyl acetate = 10:1, Rf = 0.6). ¹H NMR (500 MHz, CDCl₃) δ 7.39 – 7.20 (m, 5H, C₆H₅), 3.47 (d, *J* = 2.4 Hz, 2H, CH₂), 3.00 (t, *J* = 7.1 Hz, 2H, CH₂), 2.85 (t, *J* = 7.1 Hz, 2H, CH₂), 2.23 (t, *J* = 2.4 Hz, 1H, NH), 1.54 (s, 1H, CH).



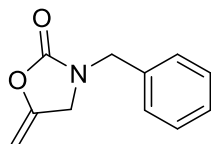
1g

Yellow oil has been obtained after being purified by column chromatography on silica gel (eluting with PE/Ethyl acetate = 5:1, Rf = 0.3). ¹H NMR (500 MHz, CDCl₃) δ 3.43 (d, *J* = 2.4 Hz, 2H, CH₂), 2.63 (s, 1H, CH), 2.17 (t, *J* = 2.4 Hz, 1H, NH), 1.85 – 1.80 (m, 2H, C₆H₁₁), 1.74 – 1.67 (m, 2H, C₆H₁₁), 1.60 (d, *J* = 12.7 Hz, 2H, C₆H₁₁), 1.29 – 1.01 (m, 5H, C₆H₁₁).



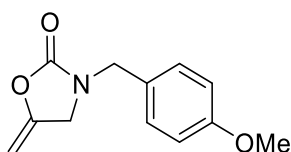
1k

Yellow oil has been obtained after being purified by column chromatography on silica gel (eluting with PE/Ethyl acetate = 5:1, Rf = 0.5). ¹H NMR (500 MHz, CDCl₃) δ 7.32 – 7.18 (m, 1H, CH), 6.96 (dd, *J* = 7.2, 3.0, 1.8 Hz, 2H, CH), 4.08 (d, *J* = 3.2 Hz, 2H, CH₂), 3.56 – 3.39 (m, 2H, CH₂), 2.28 (t, *J* = 2.4 Hz, 1H, NH), 1.77 (s, 1H, CH).



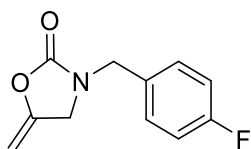
2a

Yellow oil (82.3 mg, 97%) has been obtained after being purified by column chromatography on silica gel (eluting with PE/Ethyl acetate = 10:1, R_f = 0.4). ¹H NMR (500 MHz, CDCl₃) δ 7.46 – 7.20 (m, 5H, C₆H₅), 4.72 (d, *J* = 2.9 Hz, 1H, C=CH₂), 4.45 (s, 2H, CH₂), 4.23 (d, *J* = 3.1 Hz, 1H, C=CH₂), 4.01 (t, *J* = 2.4 Hz, 2H, CH₂).



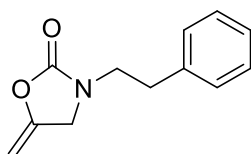
2b

Yellow oil (84 mg, 77%) has been obtained after being purified by column chromatography on silica gel (eluting with PE/Ethyl acetate = 10:1, R_f = 0.3). ¹H NMR (500 MHz, CDCl₃) δ 7.21 – 7.16 (m, 2H, C₆H₄), 6.89 – 6.84 (m, 2H, C₆H₄), 4.70 (dd, *J* = 5.6, 2.7 Hz, 1H, C=CH₂), 4.39 (s, 2H, CH₂), 4.21 – 4.22 (m, 1H, C=CH₂), 3.99 (t, *J* = 2.4 Hz, 2H, CH₂), 3.79 (s, 3H, CH₃).



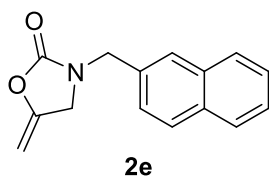
2c

Yellow oil (88.2 mg, 85%) has been obtained after being purified by column chromatography on silica gel (eluting with PE/Ethyl acetate = 10:1, R_f = 0.4). ¹H NMR (500 MHz, CDCl₃) δ 7.27 – 7.21 (m, 2H, C₆H₄), 7.02 (dd, *J* = 12.0, 5.3 Hz, 2H, C₆H₄), 4.71 (dd, *J* = 5.5, 2.7 Hz, 1H, C=CH₂), 4.41 (s, 2H, CH₂), 4.24 (dd, *J* = 5.1, 2.2 Hz, 1H, C=CH₂), 4.01 (t, *J* = 2.3 Hz, 2H, CH₂).

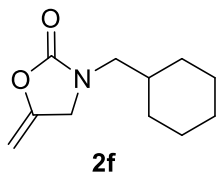


2d

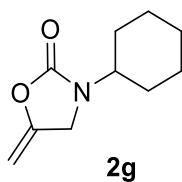
Yellow oil (91 mg, 90%) has been obtained after being purified by column chromatography on silica gel (eluting with PE/Ethyl acetate = 10:1, Rf = 0.3). ¹H NMR (500 MHz, CDCl₃) δ 7.37 – 7.19 (m, 5H, C₆H₅), 4.76 – 4.67 (m, 1H, C=CH₂), 4.27 – 4.20 (m, 1H, C=CH₂), 4.01 (t, *J* = 2.2 Hz, 2H, CH₂), 3.57 (dd, *J* = 1.6 Hz, 2H, CH₂), 2.91 (t, *J* = 7.2 Hz, 2H, CH₂).



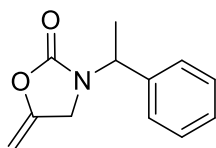
Yellow solid (97.6 mg, 81.7%) has been obtained after being purified by column chromatography on silica gel (eluting with PE/Ethyl acetate = 5:1, Rf = 0.3). ¹H NMR (500 MHz, CDCl₃) δ 7.88 – 7.81 (m, 3H, C₁₀H₇), 7.72 (s, 1H, C₁₀H₇), 7.54 – 7.46 (m, 2H, C₁₀H₇), 7.40 (dd, *J* = 8.4, 1.7 Hz, 1H, C₁₀H₇), 4.74 (dd, *J* = 5.7, 2.6 Hz, 1H, C=CH₂), 4.62 (s, 2H, CH₂), 4.22 (dt, *J* = 3.1, 2.2 Hz, 1H, C=CH₂), 4.03 (t, *J* = 2.4 Hz, 2H, CH₂).



Yellow oil (78.4 mg, 80%) has been obtained after being purified by column chromatography on silica gel (eluting with PE/Ethyl acetate = 5:1, Rf = 0.3). ¹H NMR (500 MHz, CDCl₃) δ 4.68 (dd, *J* = 5.5, 2.7 Hz, 1H, C=CH₂), 4.24 (dd, *J* = 5.2, 2.2 Hz, 1H, C=CH₂), 4.13 (t, *J* = 2.4 Hz, 2H, CH₂), 3.07 (d, *J* = 7.4 Hz, 2H, CH₂), 1.71 – 1.61 (m, 5H, C₆H₁₁), 1.16 (d, *J* = 9.4 Hz, 4H, C₆H₁₁), 0.93 (s, 2H, C₆H₁₁).

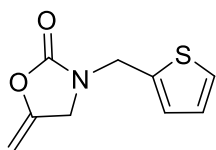


Yellow oil (85.2 mg, 94%) has been obtained after being purified by column chromatography on silica gel (eluting with PE/Ethyl acetate = 5:1, R_f = 0.2). $^1\text{H NMR}$ (500 MHz, CDCl_3) δ 4.69 (dd, J = 5.5, 2.7 Hz, 1H, $\text{C}=\text{CH}_2$), 4.25 (dd, J = 5.2, 2.2 Hz, 1H, $\text{C}=\text{CH}_2$), 4.11 (t, J = 2.4 Hz, 2H, CH_2), 3.69 (s, 1H, C_6H_{11}), 1.79 (d, J = 8.4 Hz, 4H, C_6H_{11}), 1.65 (d, J = 13.0 Hz, 1H, C_6H_{11}), 1.38 – 1.28 (m, 4H, C_6H_{11}), 1.06 (dd, J = 3.0 Hz, 1H, C_6H_{11}).



2i

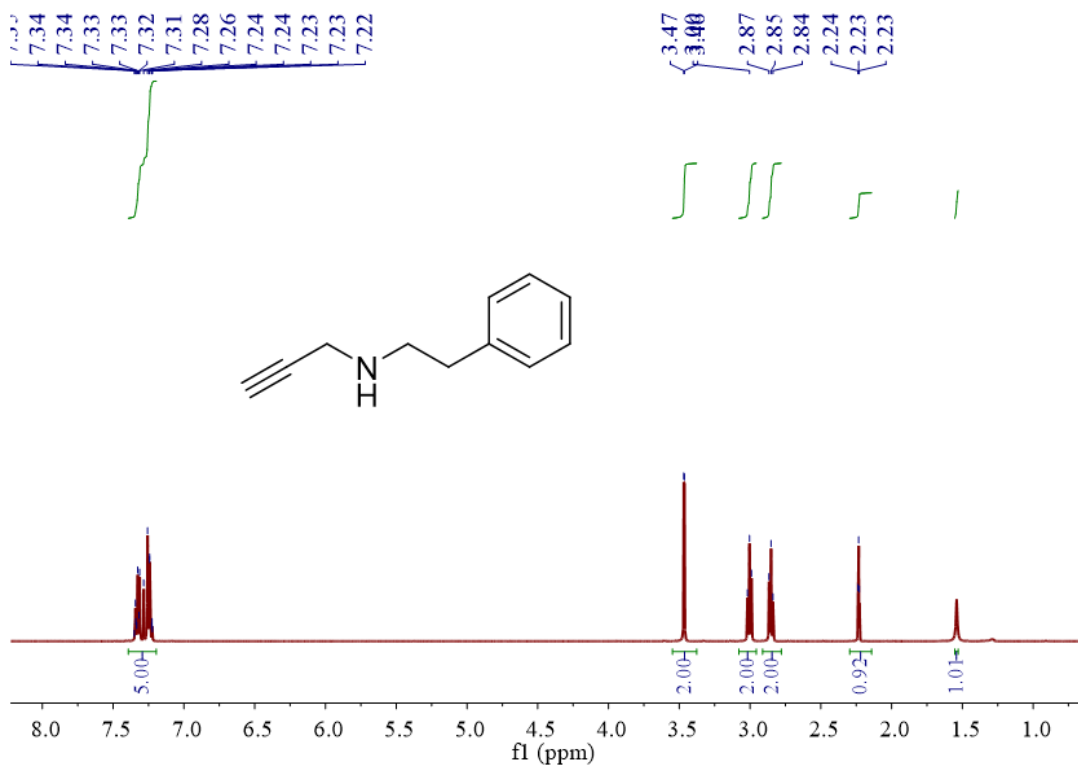
Yellow oil (67.2 mg, 66%) has been obtained after being purified by column chromatography on silica gel (eluting with PE/Ethyl acetate = 10:1, R_f = 0.5). $^1\text{H NMR}$ (500 MHz, CDCl_3) δ 7.39 – 7.29 (m, 5H, C_6H_5), 5.26 (d, J = 7.1 Hz, 1H, CH), 4.70 (dd, J = 5.6, 2.7 Hz, 1H, $\text{C}=\text{CH}_2$), 4.21 (dt, J = 3.1, 2.2 Hz, 1H, $\text{C}=\text{CH}_2$), 4.10 (dt, J = 14.2, 2.4 Hz, 1H, CH_2), 3.76 (dt, J = 2.4 Hz, 1H, CH_2), 1.59 (d, J = 7.1 Hz, 3H, CH_3).



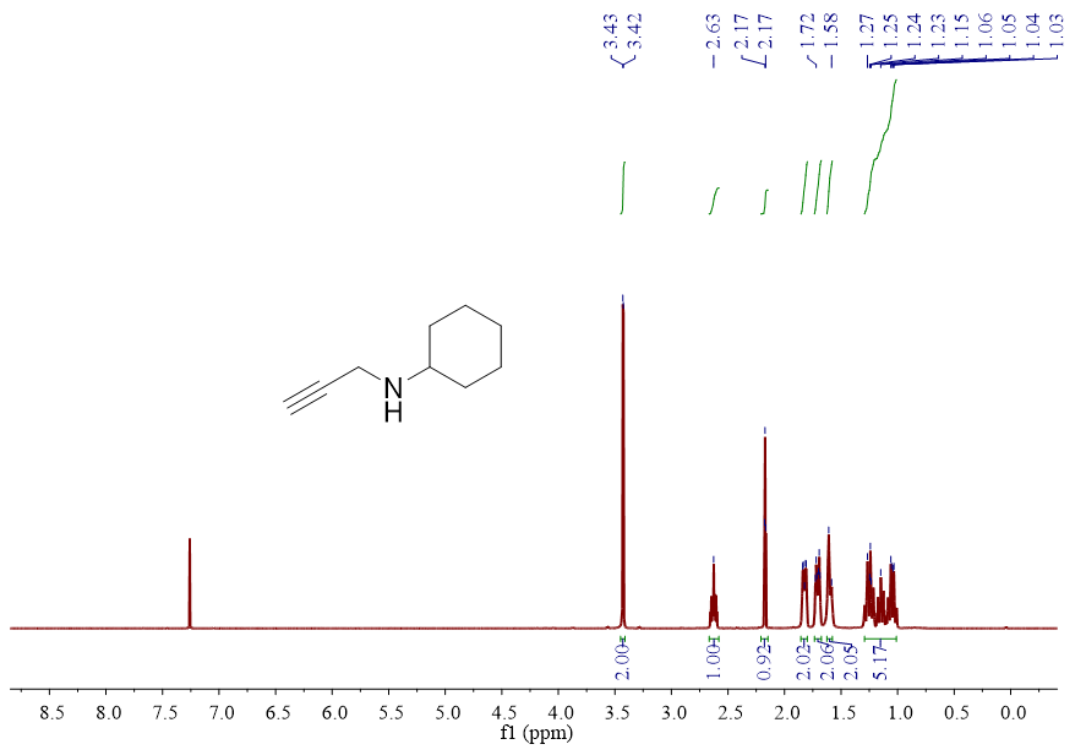
2k

Yellow oil (89.2 mg, 92%) has been obtained after being purified by column chromatography on silica gel (eluting with PE/Ethyl acetate = 5:1, R_f = 0.5). $^1\text{H NMR}$ (500 MHz, CDCl_3) δ 7.31 – 7.23 (m, 1H, $\text{C}_4\text{H}_3\text{S}$), 7.03 – 6.93 (m, 2H, $\text{C}_4\text{H}_3\text{S}$), 4.72 (dd, J = 5.7, 2.7 Hz, 1H, $\text{C}=\text{CH}_2$), 4.63 (s, 2H, CH_2), 4.25 (dd, J = 0.9 Hz, 1H, $\text{C}=\text{CH}_2$), 4.09 (t, J = 2.4 Hz, 2H, CH_2).

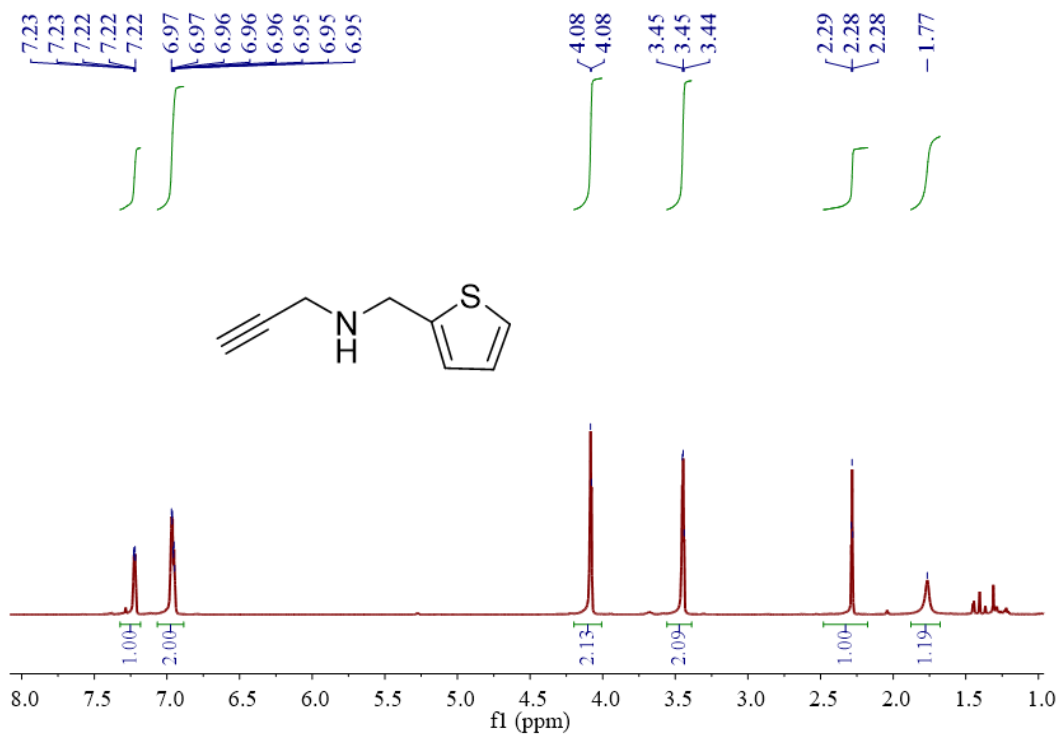
NMR spectra of substrates and products



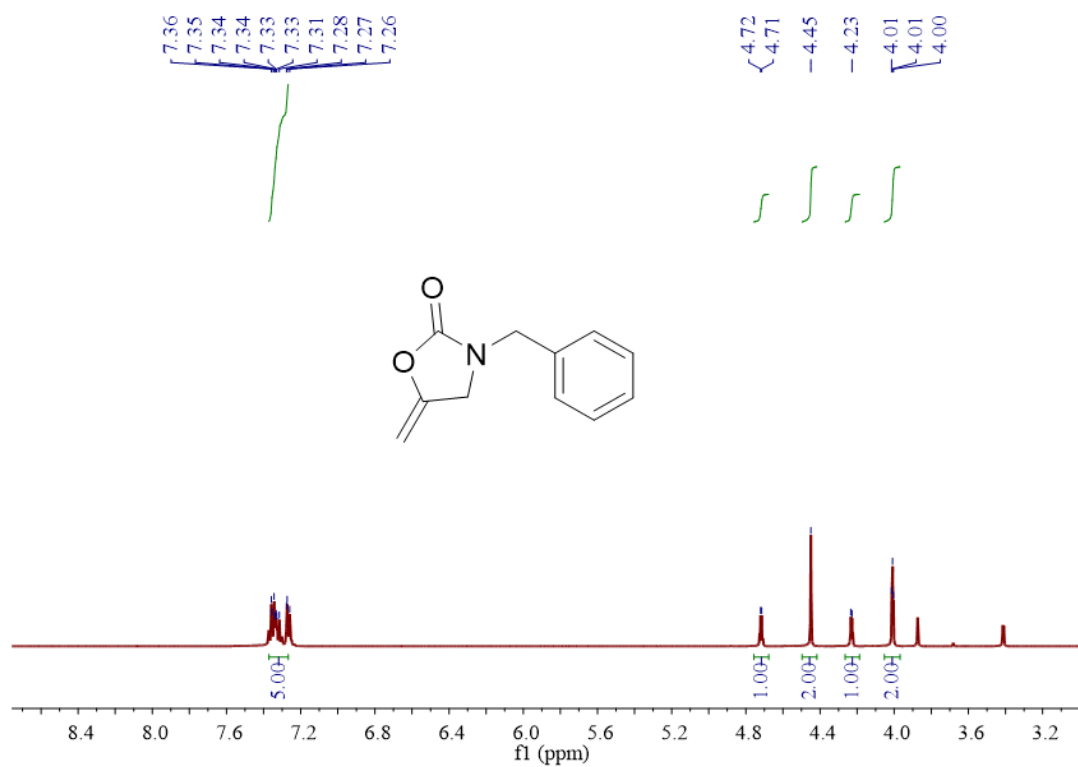
¹H NMR (500 MHz, CDCl₃) spectrum of **1d**.



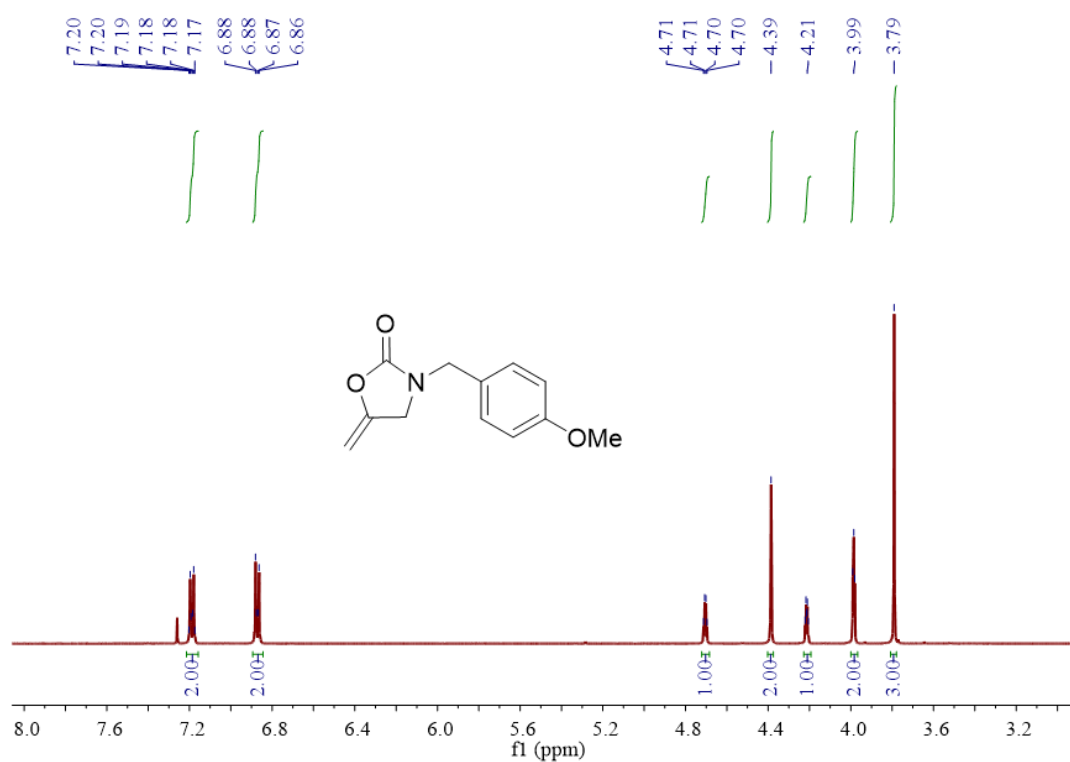
¹H NMR (500 MHz, CDCl₃) spectrum of **1g**.



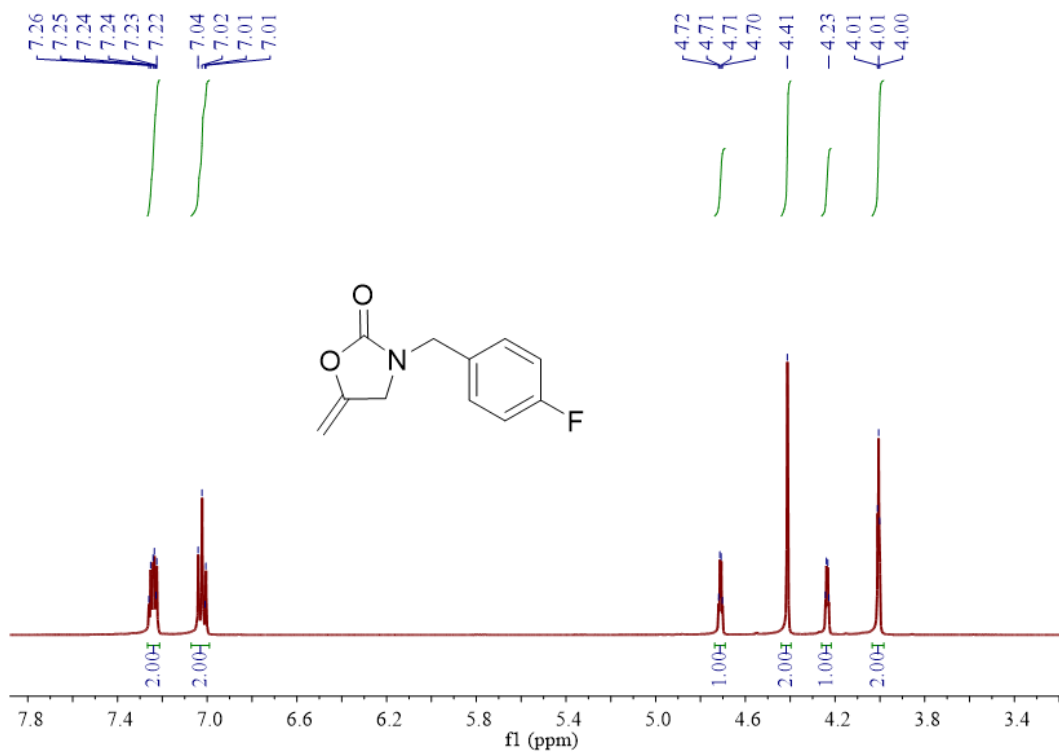
¹H NMR (500 MHz, CDCl₃) spectrum of **1k**.



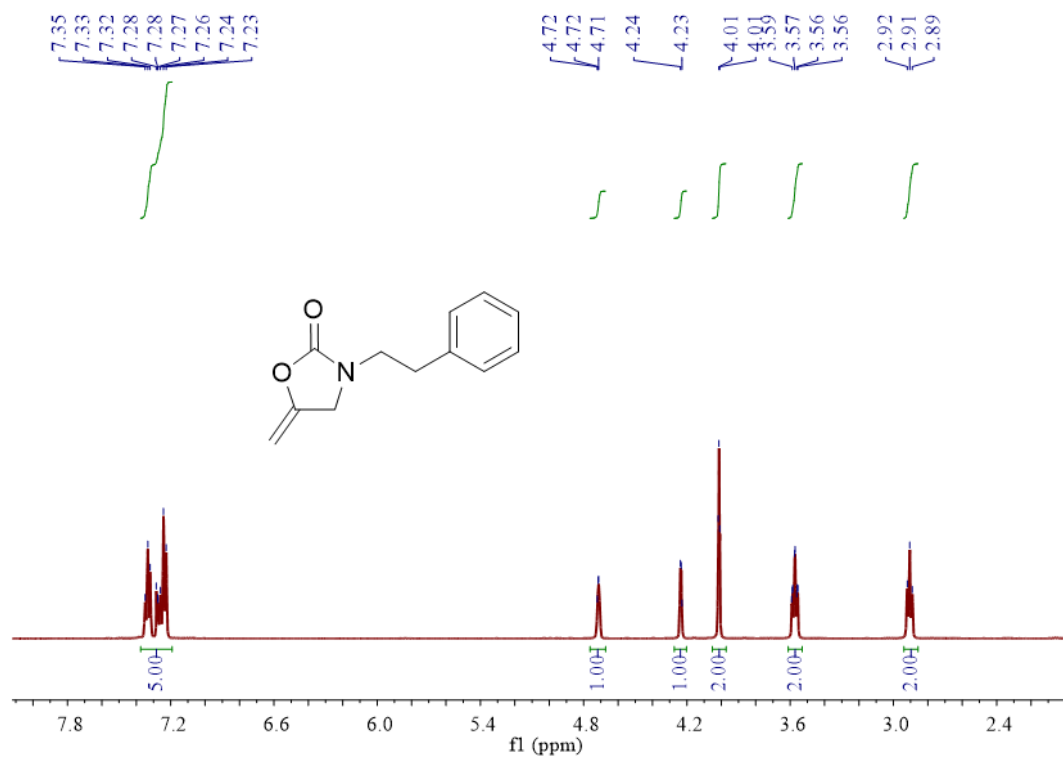
¹H NMR (500 MHz, CDCl₃) spectrum of **2a**.



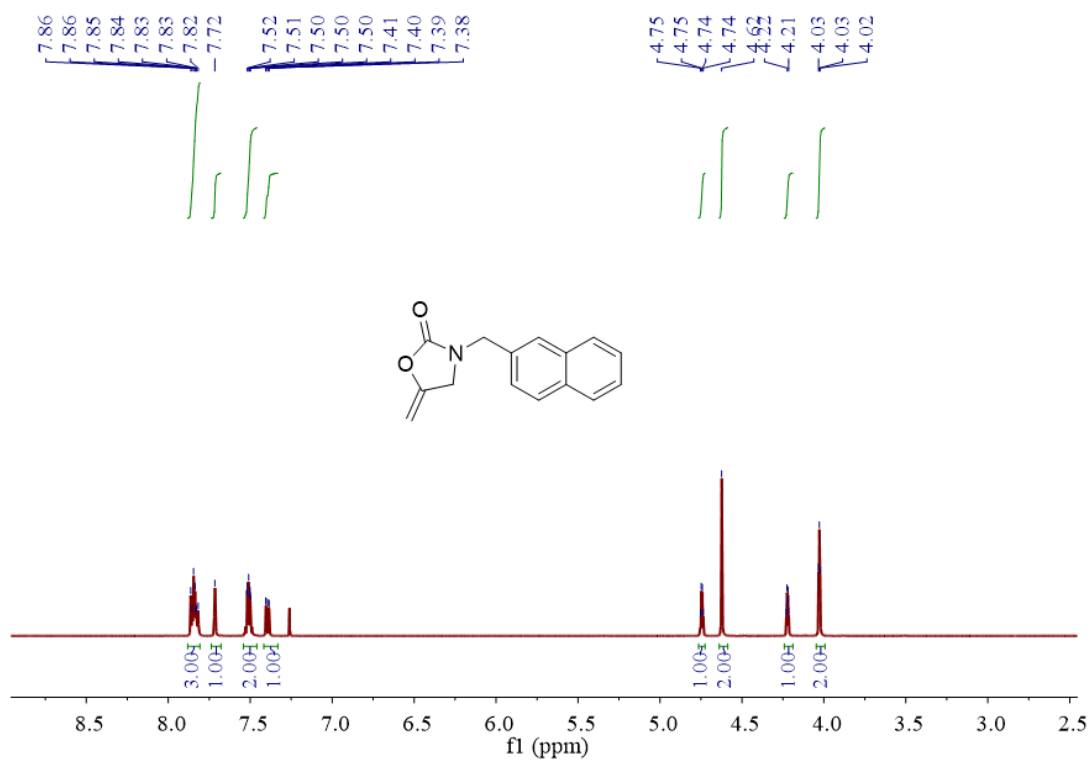
¹H NMR (500 MHz, CDCl₃) spectrum of **2b**.



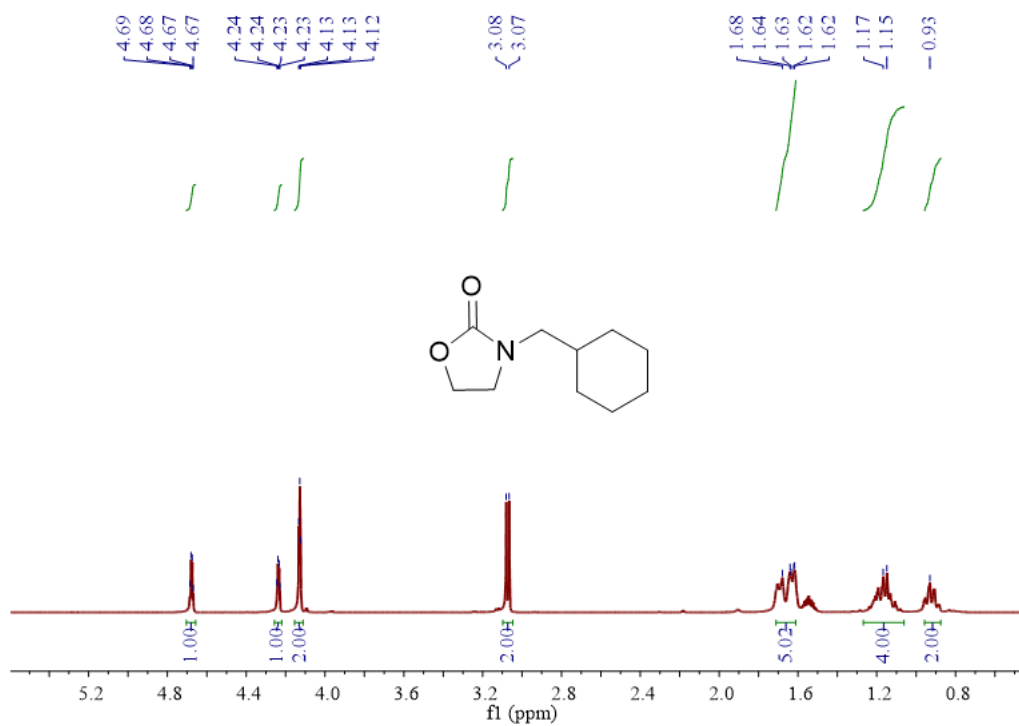
$^1\text{H NMR}$ (500 MHz, CDCl_3) spectrum of **2c**.



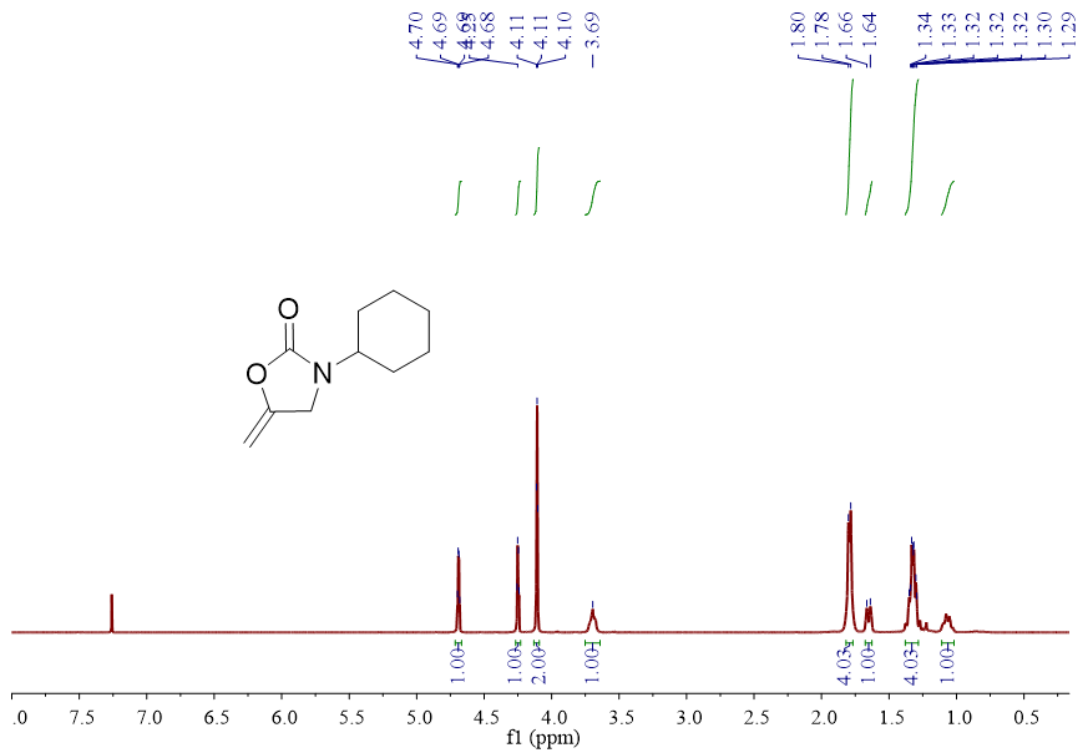
$^1\text{H NMR}$ (500 MHz, CDCl_3) spectrum of **2d**.



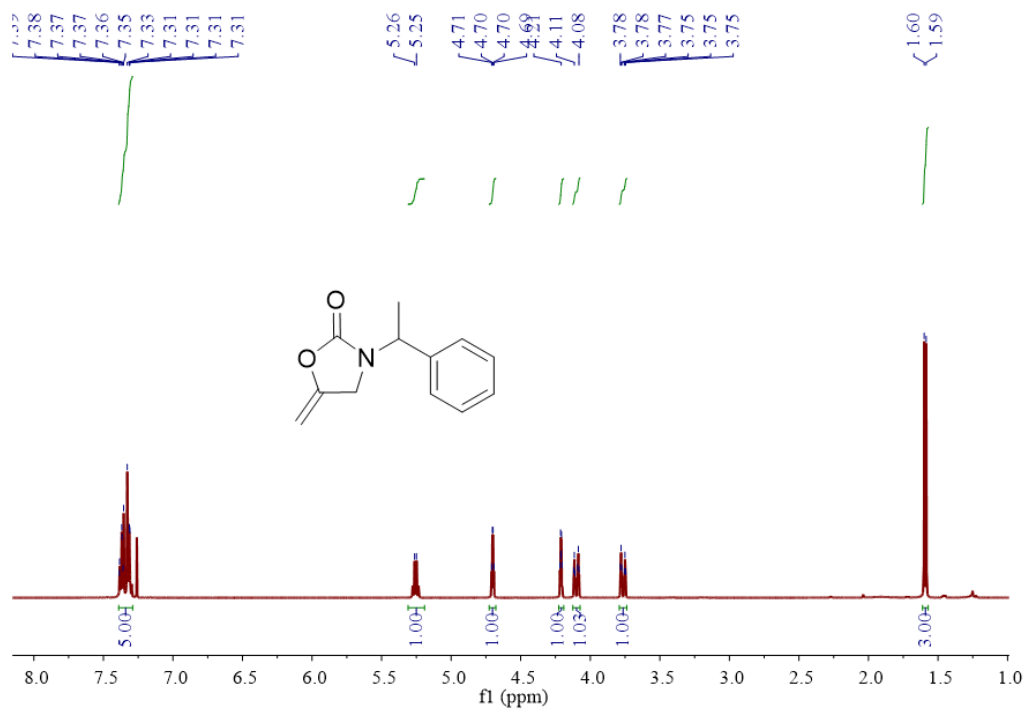
¹H NMR (500 MHz, CDCl₃) spectrum of **2e**.¹



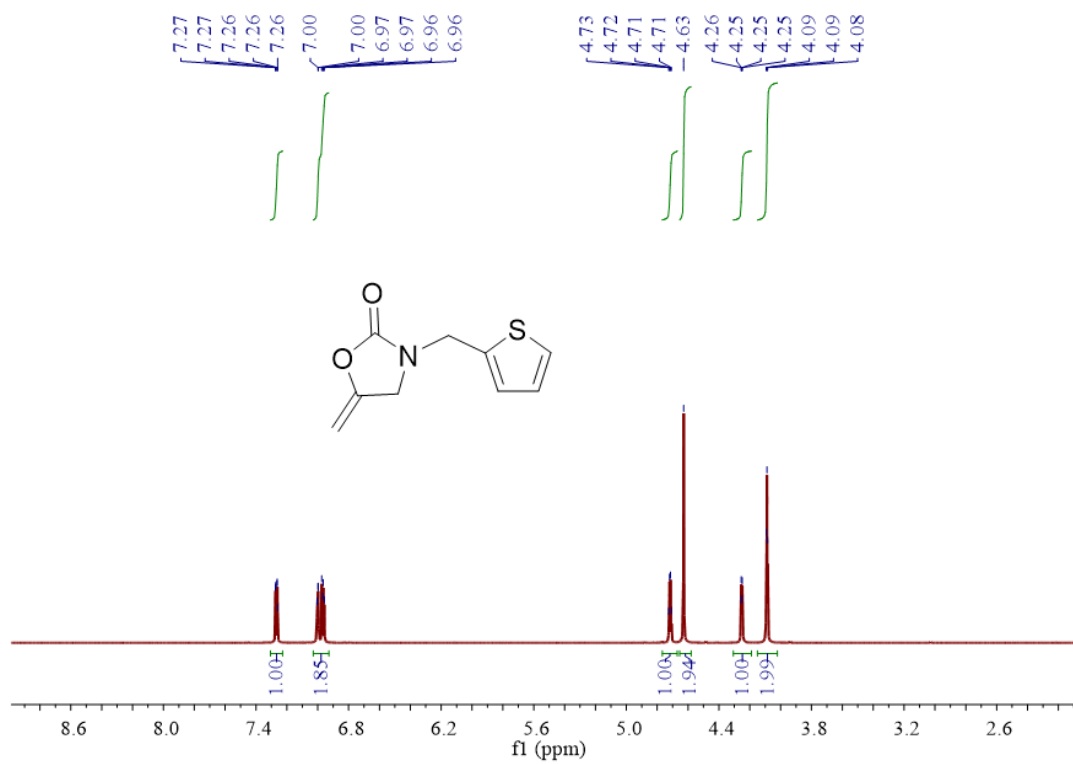
¹H NMR (500 MHz, CDCl₃) spectrum of **2f**.



¹H NMR (500 MHz, CDCl₃) spectrum of 2g.



¹H NMR (500 MHz, CDCl₃) spectrum of 2i.



¹H NMR (500 MHz, CDCl₃) spectrum of **2k**.

Reference

1. Zhao, X.; Qin, B.-B.; He, T.; Wang, H.-P.; Liu, J. Stable Pyrene-Based Metal–Organic Framework for Cyclization of Propargylic Amines with CO₂ and Detection of Antibiotics in Water. *Inorg. Chem.* **2023**, *62*, 18553–18562.
2. Liu, X.; Wang, M.-Y.; Wang, S.-Y.; Wang, Q.; He, L.-N. In Situ Generated Zinc (II) Catalyst for Incorporation of CO₂ into 2-Oxazolidinones with Propargylic Amines at Atmospheric Pressure, *ChemSusChem*, **2017**, *10*, 1210–1216.
3. Zhang, C.-H.; Hu, T.-D.; Zhai, Y.-T.; Zhang, Y.-X.; Wu, Z.-L. Stepwise engineering of the pore environment within metal–organic frameworks for green conversion of CO₂ and propargylic amines, *Green Chem.* **2023**, *25*, 1938- 1947.